Calculations of stopping powers of 100 eV–30 keV electrons in 31 elemental solids

S. Tanuma,[1] C. J. Powell,[2,a)] and D. R. Penn[2]
[1]*Materials Analysis Station, National Institute for Materials Science, 1-2-1 Sengen, Tsukuba, Ibaraki 305-0047, Japan*
[2]*National Institute of Standards and Technology, Gaithersburg, Maryland 20899-8370, USA*

(Received 1 November 2007; accepted 3 January 2008; published online 19 March 2008)

We present calculated electron stopping powers (SPs) for 31 elemental solids (Li, Be, glassy C, graphite, diamond, Na, Mg, K, Sc, Ti, V, Fe, Y, Zr, Nb, Mo, Ru, Rh, In, Sn, Cs, Gd, Tb, Dy, Hf, Ta, W, Re, Os, Ir, and Bi). These SPs were determined with an algorithm previously used for the calculation of electron inelastic mean free paths and from energy-loss functions (ELFs) derived from experimental optical data. The SP calculations were made for electron energies between 100 eV and 30 keV and supplement our earlier SP calculations for ten additional solids (Al, Si, Cr, Ni, Cu, Ge, Pd, Ag, Pt, and Au). Plots of SP versus atomic number for the group of 41 solids show clear trends. Multiple peaks and shoulders are seen that result from the contributions of valence-electron and various inner-shell excitations. Satisfactory agreement was found between the calculated SPs and values from the relativistic Bethe SP equation with recommended values of the mean excitation energy (MEE) for energies above 10 keV. We determined effective MEEs versus maximum excitation energy from the ELFs for each solid. Plots of effective MEE versus atomic number showed the relative contributions of valence-electron and different core-electron excitations to the MEE. For a maximum excitation energy of 30 keV, our effective MEEs agreed well for Be, graphite, Na, Al, and Si with recommended MEEs; a difference for Li was attributed to sample oxidation in the SP measurements for the recommended MEE. Substantially different effective MEEs were found for the three carbon allotropes (graphite, diamond, and glassy C). © *2008 American Institute of Physics*. [DOI: 10.1063/1.2891044]

INTRODUCTION

The electron stopping power (SP) is an important parameter in radiation dosimetry[1] and in the modeling of electron transport in matter for many other applications. For example, the SP has been used in Monte Carlo simulations of electron transport relevant to electron-probe microanalysis,[2–4] Auger-electron spectroscopy,[5] and dimensional metrology in the scanning electron microscope.[6] The Bethe SP equation[7–9] has been used extensively for energies where it is expected to be valid (i.e., at energies much larger than the largest K-shell binding energy in the material of interest), but there is a scarcity of data at lower energies. SPs calculated from the Bethe equation are available from a NIST database for electron energies of 10 keV and above.[10]

We report calculated SPs for 100 eV–30 keV electrons in 31 elemental solids (Li, Be, glassy C, graphite, diamond, Na, Mg, K, Sc, Ti, V, Fe, Y, Zr, Nb, Mo, Ru, Rh, In, Sn, Cs, Gd, Tb, Dy, Hf, Ta, W, Re, Os, Ir, and Bi). These SPs were calculated from experimental optical data using an approach based on Penn's algorithm for the calculation of electron inelastic mean free paths (IMFPs).[11] We have previously published SPs for ten other elemental solids (Al, Si, Cr, Ni, Cu, Ge, Pd, Ag, Pt, and Au) using the same method.[12] SP calculations for the total group of 41 solids are feasible because the needed optical data are available.

We give a brief summary of our method for the calculation of SPs in the next section. The new SPs are presented in the following section, and then SPs for the entire group of 41 solids are discussed. We examine trends in plots of SP versus electron energy as well as evaluations of the mean excitation energy (MEE) from the optical data. The MEE is the key material-specific parameter in the Bethe SP equation.

CALCULATION OF ELECTRON SPs

Penn[11] has described an algorithm for the calculation of electron IMFPs from a model dielectric function $\varepsilon(q,\omega)$, a function of momentum transfer q and energy loss $\hbar\omega$.[13] The differential inelastic-scattering cross section, per atom or molecule, for an electron of kinetic energy $E=m_0v^2/2$ in an infinite medium is

$$\frac{d^2\sigma}{dqd\omega}=\frac{m_0e^2}{\pi N\hbar E}\,\mathrm{Im}\left[\frac{-1}{\varepsilon(q,\omega)}\right]\frac{1}{q}, \tag{1}$$

where m_0 is the electronic rest mass, e is the electronic charge, N is the density of atoms or molecules per unit volume, and $\mathrm{Im}[-1/\varepsilon(q,\omega)]$ is the energy-loss function (ELF). The dependence of the ELF on ω can be obtained from experimental optical data for the material of interest for $q=0$, and the dependence of the ELF on q can be obtained from an appropriate theoretical model.[13] In our work, we utilized the Lindhard[14] dielectric function to describe the q dependence of the ELF.

a)Electronic mail: cedric.powell@nist.gov.

The SP is proportional to an integral of $\mathrm{Im}[-1/\varepsilon(q,\omega)] \times(\omega/q)$ over the kinematically allowed regions of q and ω.[1,15] We have calculated the SP, S, from optical data using the Penn single-pole approximation,[11]

$$S=\frac{1}{\pi a_0 E}\int_0^{\infty}\omega_p\,\mathrm{Im}\left[\frac{-1}{\varepsilon(\omega_p)}\right]d\omega_p\int_{q^-}^{q^+}\frac{dq}{q\omega_p(q)} \times\int_0^{E-E_f}(\hbar\omega)d(\hbar\omega)\delta[\omega-\omega_p(q)], \tag{2a}$$

where

$$\omega_p^2(q)=\omega_p^2+\tfrac{1}{3}[v(\omega_p)q]^2+(\hbar q^2/2m_0)^2, \tag{2b}$$

$$q^{\pm}=(\sqrt{2m_0E}/\hbar)[1\pm\sqrt{1-(\hbar\omega/E)}], \tag{2c}$$

$v(\omega_p)$ is the Fermi velocity of a free-electron gas with plasma frequency ω_p, a_0 is the Bohr radius, and E_F is the Fermi energy. After performing two integrations, the SP becomes

$$S=\frac{1}{\pi a_0 E}\int_0^{\infty}(\hbar\omega_p)\mathrm{Im}\left[\frac{-1}{\varepsilon(\omega_p)}\right]\ln\left(\frac{q_{\max}}{q_{\min}}\right)d(\hbar\omega_p), \tag{3}$$

where $q_{\min}$ and $q_{\max}$ can be determined from equations given by Penn.[11] SPs can be computed from Eq. (3) using values of $\mathrm{Im}[-1/\varepsilon(0,\omega)]$ obtained from optical constants in the literature, as described elsewhere.[16,17] We evaluated the internal consistency of the sets of $\mathrm{Im}[-1/\varepsilon(0,\omega)]$ data using two useful sum rules (the f-sum rule and the perfect-screening sum rule);[16–18] these sum rules were satisfied with root-mean-square errors of 7.4% and 9.2%, respectively.[16,17] Our SP calculations for Ti were based on an improved set of ELF data obtained from Ref. 19 for photon energies between 0.0062 and 25.0 eV, from Ref. 20 for photon energies between 25.5 and 99.0 eV, and from Ref. 21 for photon energies between 99.26 and 30 000 eV. For this Ti data set, the f-sum and perfect-screening sum-rule errors were −5.8% and −1.6%, respectively (compared to −18% and 0%, respectively, for the original data set[16]).

Several additional factors limit the reliability of our calculated SPs. First, the Lindhard dielectric model is expected to provide a useful approximation for the q dependence of valence-electron excitations in free-electron-like solids but will be less reliable for non-free-electron-like solids. First, the ELF for $q=0$, $\mathrm{Im}[-1/\varepsilon(0,\omega)]$ in the Lindhard model, is equated with $\mathrm{Im}[-1/\varepsilon(\omega)]$ from the optical data. Deviations from the q dependence of the ELF from the Lindhard model should thus not greatly affect the calculated SPs for small q (where $\mathrm{Im}[-1/\varepsilon(0,\omega)]$ is relatively large); for large q, the deviations will not be significant since $\mathrm{Im}[-1/\varepsilon(0,\omega)]$ is relatively small. Second, the use of the Lindhard model for describing the q dependence of core-electron excitations, however, is less likely to be correct. Despite this limitation, a more detailed calculation of the Al $2p$ and Mo $3d$ inelastic-scattering cross sections showed good agreement with those found using the Lindhard model if the integrations of Eq. (1) were made over sufficiently large ranges of energy transfer, typically greater than 100 eV for Al and 200 eV for Mo;[22] in the present work, the maximum energy transfers were generally an order of magnitude larger than these limits. We also made comparisons of SPs from the Penn model with values obtained from $q_{\max}$ calculated from the largest reasonable energy transfer, here assumed to be $E/2$. These calculations were made for six selected solids (Mg, Al, Fe, Mo, Ir, and Au) and showed that SPs from the two approaches agreed to better than 5%. At lower energies, SPs from the Penn algorithm exceeded values from the other model by between 4% and 10%. Third, no account has been taken of exchange effects in inelastic scattering. Comparisons of our calculated SPs for Al, Si, Cu, and Au with those of Fernandez-Varea *et al.*[23] who included an exchange correction in their algorithm showed close agreement for energies greater than about 500 eV.[12] This agreement indicates that the exchange correction introduced by these authors for inner-shell excitations must be relatively small or otherwise compensated by some other difference in their algorithm and ours. At lower energies, there were small differences in the energies for the SP maximum, the values of the maximum SP, and/or in the peak shapes.[12] The Ochkur[24] exchange correction has been used in some SP calculations, and Tan *et al.*[25] have found that use of this correction leads to average decreases in SPs of about 28%, 9%, and 9% at energies of 100, 1000, and 10 000 eV, respectively, for a group of ten organic compounds. Nevertheless, we point out that our calculated SPs (Ref. 12) (made without any exchange correction) for Al, Si, Cr, Ni, Cu, Ge, Pd, Ag, and Pt agreed reasonably with available experimental data, as indicated in more detail below. Finally, we note that the Penn single-pole approximation used in our SP calculations is less accurate than the full Penn algorithm for electron energies less than about 300 eV. For IMFPs, the differences between IMFPs calculated from the single-pole approximation at energies between 50 and 330 eV are generally less than 7% of those from the full Penn algorithm.[12] We therefore believe that use of the simpler single-pole approximation is satisfactory for energies larger than 100 eV.

RESULTS

We calculated SPs for the 31 elemental solids at electron energies between 10 eV and 30 keV. These SPs were calculated at equal intervals on a logarithmic energy scale corresponding to increases of 10%. This choice was made to facilitate data display and analysis.

The solid lines in Figs. 1–6 show plots of the calculated SPs as a function of energy for the 31 solids considered here and for the earlier group of ten solids[12] to show systematic trends in the shapes of the plots as a function of atomic number. We include data in these plots for energies less than 100 eV to illustrate trends, but these data are not considered reliable, as discussed above. Calculated SPs for energies between 99.5 and 29 732.6 eV are shown in Table I for the group of 31 solids. The calculated SPs in Figs. 1–6 show systematic trends with atomic number. Sometimes, a single maximum is observed in the SP versus energy curves, sometimes secondary structures or multiple maxima are observed, and there are varying widths of the main maximum that occurs generally at energies between 10 and 300 eV. These trends are discussed further below.

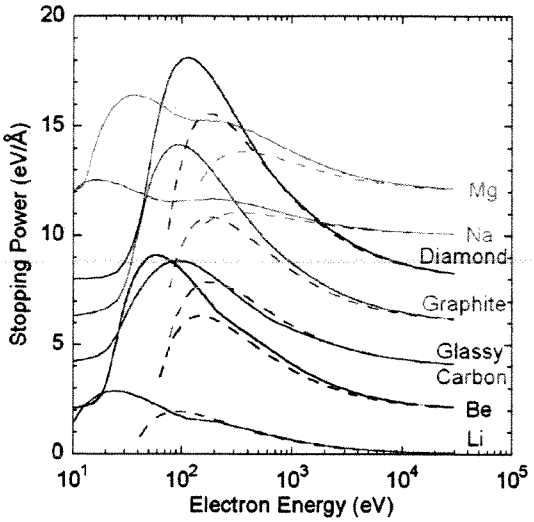

FIG. 1. (Color online) The solid lines show calculated SPs for Li, Be, glassy carbon, graphite, diamond, Na, and Mg as a function of electron kinetic energy E. The dashed lines show SPs calculated from the relativistic Bethe equation [Eq. (5)]. For clarity, the results for Be and successive elements have been moved upward in increments of 2 eV/Å

The dashed lines in Figs. 1–6 show SPs calculated from the relativistic Bethe equation,[1,7–9]

$$S = \frac{2\pi r_e^2 m_0 c^2}{u\beta^2}\frac{Z\rho}{A}[\ln(T/I)^2 + \ln(1+\tau/2) + F(\tau) - \delta], \quad (4a)$$

where

$$F(\tau) = (1-\beta^2)[1 + \tau^2/8 - (2\tau+1)\ln 2], \quad (4b)$$

$r_e = 2.817\,940\,289\,4 \times 10^{-15}$ m is the classical electron radius,[26] $m_0c^2 = 0.510\,998\,910$ MeV is the electron rest energy,[26] $u = 1.660\,538\,782 \times 10^{-27}$ kg is the atomic mass unit,[26] β is the electron velocity divided by the velocity of light, $\tau = T/m_0c^2$ is the ratio of the electron relativistic energy to its rest energy, and δ is a density-effect correction. We have assumed δ to be zero here since its calculation is difficult and its inclusion leads, for our energy range, to a correction of less than 0.3%.[1] The other terms in Eq. (4a) are parameters describing the material of interest: Z is the atomic number, ρ is the density, A is the atomic weight, and I is the MEE. We note that Eq. (4a) does not include a so-called shell correction to the SP; this omission is discussed below.

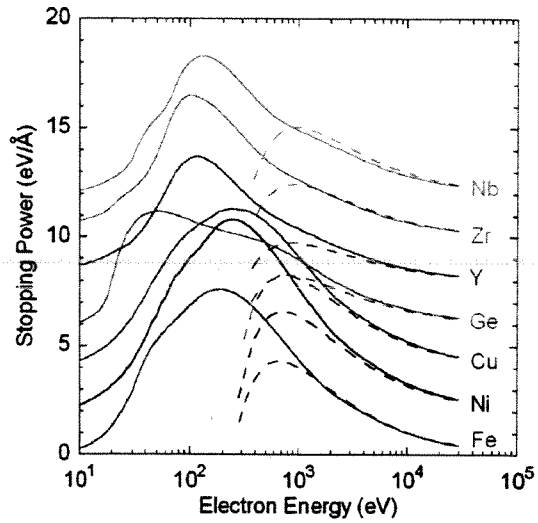

FIG. 3. (Color online) Same as Fig. 1 except for Fe, Ni, Cu, Ge, Y, Zr, and Nb.

With values of the constants inserted, Eq. (4a) becomes

$$S = \frac{392.29Z\rho}{EA}[\ln(T/I)^2 + \ln(1+\tau/2) + F(\tau)] \quad (\text{in eV/Å}) \quad (5)$$

if the density is expressed in g/cm^3 and E and T in eV. At nonrelativistic energies, $\tau \to 0$, $\ln(1+\tau/2) \to 0$, $F(\tau) \to 1 - \ln 2$, and $T \approx E$. Equation (5) then becomes

$$S = \frac{784.6Z\rho}{EA}\ln\left(\frac{1.166E}{I}\right) \quad (\text{in eV/Å}). \quad (6)$$

We have calculated SPs from Eq. (5) using the values of I listed in Table 4.3 of Ref. 1. Most of the needed MEE values

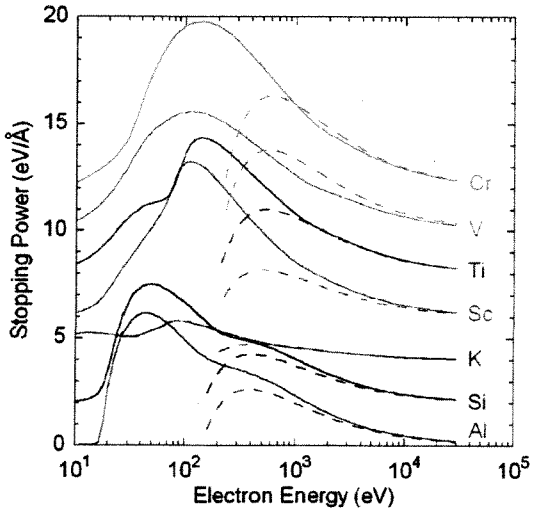

FIG. 2. (Color online) Same as Fig. 1 except for Al, Si, K, Sc, Ti, V, and Cr.

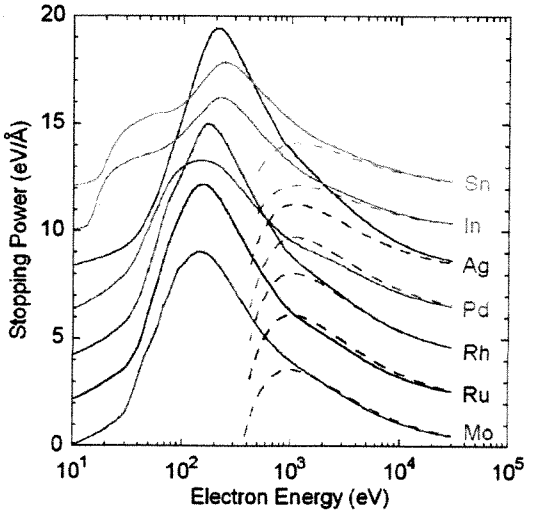

FIG. 4. (Color online) Same as Fig. 1 except for Mo, Ru, Rh, Pd, Ag, In, and Sn.

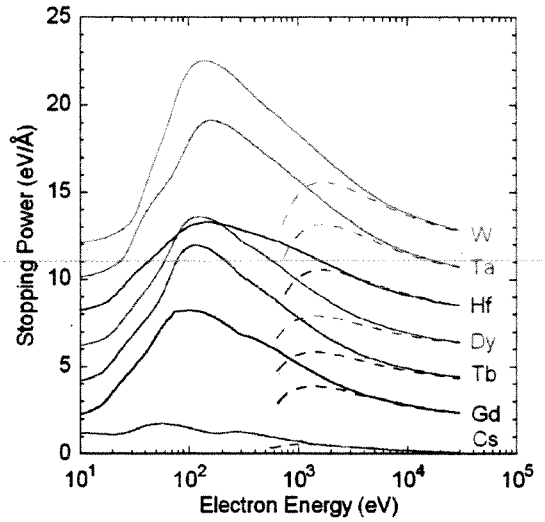

FIG. 5. (Color online) Same as Fig. 1 except for Cs, Gd, Tb, Dy, Hf, Ta, and W.

were obtained from measurements of proton SPs and ranges, but some values (for Na, Mg, K, Y, Ru, Cs, Tb, Dy, Hf, Rh, Os, and Bi) were determined by interpolation.[1] We have used the same MEE values for glassy C and diamond as that listed for graphite (78 eV) (Ref. 1) although, as we show below, larger MEEs are more appropriate for these two solids.

SPs from Eq. (5) are shown in Figs. 1–6 from the minimum energies for which S is positive to our upper limit of 30 keV. While the Bethe equation is not expected to be valid at energies less than the K-shell binding energy, Figs. 1–6 illustrate the energy regions over which our calculated SPs agree reasonably with those from Eq. (5). We discuss the energy range for validity of the Bethe SP equation in more detail below.

SP calculations at electron energies less than 30 keV have been made previously only for a limited number of elemental solids such as Al, Si, Cu, Ge, Ag, and Au.[12,27] The SP versus energy curves typically show a single maximum although evidence for other structure can be seen in calculated SPs for Al and Cu. Our calculated SPs in Figs. 1–6 show clear trends in the shapes of the curves as a function of Z. Multiple peaks and shoulders are seen that result from the separate contributions of valence-electron excitations and various inner-shell excitations to the total SP. For Li and Be in Fig. 1, for example, separate structures are seen that result from valence-electron excitations (at low electron energies) and from K-shell excitations. With increasing Z, these structures overlap until, for Na, Mg, Al, and Si, separate structures are clearly visible (Figs. 1 and 2). Separate structures are generally seen for elements with core-electron binding energies of less than about 50 eV, such as Na (Fig. 1), Ge (Fig. 3), In and Sn (Fig. 4), Cs (Fig. 5), and Bi (Fig. 6). For other elements, a single maximum may be seen in Figs. 1–6, but the shapes and widths vary appreciably with Z. These changes are believed to be due to the varying contributions of valence-electron and different inner-shell excitations. An analysis of these trends will be reported separately.[28] Changes in the magnitudes of the SP at any energy in Figs. 1–6 are largely due to variations of bulk density (e.g., as for the SPs of glassy C, graphite, and diamond in Fig. 1).

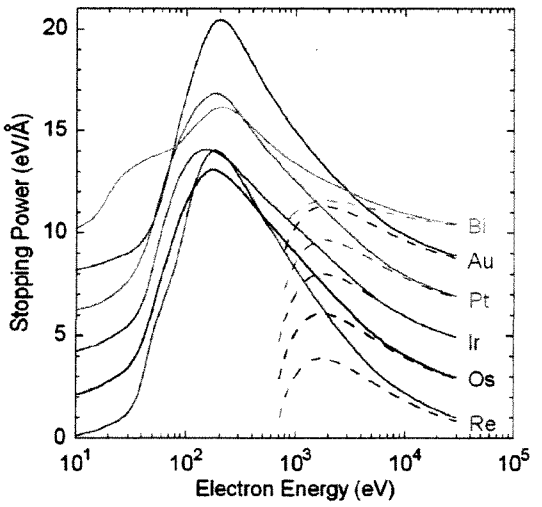

FIG. 6. (Color online) Same as Fig. 1 except for Re, Os, Ir, Pt, Au, and Bi.

DISCUSSION

Comparisons with other results

Measurements of electron SPs for electron energies less than 30 keV have been made for a relatively small number of elemental solids.[12,29] We previously compared our calculated SPs for Al, Si, Cr, Ni, Cu, Ge, Pd, Ag, Pt, and Au with SPs based on measurements of electron energy-loss spectra (EELS) of 100 or 200 keV electrons transmitted through thin specimen films, calorimetry experiments, transmission of 1 eV–4 keV electrons through thin films of Al deposited on an oxidized Al substrate, and energy distributions of 0.65 keV–10.9 keV electrons transmitted through thin Al films.[12] We found generally satisfactory agreement of our calculated SPs for some solids (Ni, Cu, Pd, and Pt) and limited agreement for other materials [Al, Si (for $E>100$ eV), Cr (except for energies between 100 and 700 eV), Ge (for $E>200$ eV), and Ag (for $E>5$ keV)]. Relatively poor agreement was found for Au. Given the spread of more than a factor of 2 in reported SPs for Al (the solid for which most measurements have been made), the degree of agreement between calculated and measured SPs was considered satisfactory. Figure 7 shows a comparison of our calculated SPs for graphite with values derived from EELS measurements;[30] very good agreement is found for $E>100$ eV.

Our calculated SPs for Al, Cu, Ag, and Au were systematically smaller than those calculated by Ashley[31] by up to 33% for $E<10$ keV.[12] These differences were believed to be mainly due to the effects of an exchange correction in Ashley's calculations. Our SPs for Cu agreed well with those calculated by Ding and Shimizu[32] with the Penn algorithm but poorer agreement, with deviations of up to 15% for $E>70$ eV, was found for Au. We found generally close agreement between our SPs for Al, Si, Cu, and Au with those calculated by Fernandez-Varea *et al.*[23] (who included an exchange correction) although their maximum SPs for Al and Cu were 10% smaller and 23% larger, respectively, than our

TABLE I. Calculated SPs for 31 elemental solids as a function of electron kinetic energy $E=m_0v^2/2$.

	Stopping power (eV/Å)							
E (eV)	Li	Be	Glassy C	Graphite	Diamond	Na	Mg	K
99.5	1.72	6.44	4.84	8.14	10.0	1.57	3.41	1.79
109.9	1.66	6.22	4.81	8.07	10.1	1.59	3.32	1.75
121.5	1.62	5.98	4.74	7.95	10.1	1.61	3.27	1.69
134.3	1.60	5.72	4.65	7.77	9.99	1.63	3.26	1.63
148.4	1.57	5.47	4.53	7.57	9.82	1.64	3.25	1.57
164.0	1.55	5.20	4.39	7.33	9.59	1.66	3.24	1.50
181.3	1.52	4.94	4.25	7.07	9.32	1.67	3.24	1.44
200.3	1.49	4.68	4.09	6.79	9.01	1.67	3.23	1.37
221.4	1.45	4.45	3.92	6.50	8.68	1.66	3.21	1.30
244.7	1.41	4.27	3.75	6.21	8.32	1.65	3.18	1.24
270.4	1.36	4.11	3.58	5.91	7.96	1.63	3.13	1.18
298.9	1.31	3.96	3.40	5.61	7.58	1.60	3.07	1.11
330.3	1.25	3.81	3.23	5.31	7.21	1.56	3.00	1.05
365.0	1.20	3.66	3.06	5.02	6.83	1.51	2.90	1.00
403.4	1.14	3.50	2.89	4.73	6.46	1.47	2.81	0.940
445.9	1.08	3.35	2.72	4.45	6.10	1.41	2.74	0.885
492.7	1.03	3.19	2.56	4.18	5.74	1.36	2.62	0.832
544.6	0.969	3.03	2.40	3.92	5.40	1.30	2.51	0.782
601.8	0.913	2.88	2.26	3.68	5.07	1.24	2.41	0.733
665.1	0.859	2.72	2.12	3.46	4.78	1.18	2.29	0.689
735.1	0.806	2.57	2.02	3.26	4.52	1.12	2.18	0.655
812.4	0.756	2.43	1.94	3.08	4.27	1.06	2.07	0.626
897.8	0.707	2.28	1.85	2.90	4.04	0.998	1.96	0.599
992.3	0.661	2.14	1.74	2.73	3.82	0.940	1.85	0.573
1 096.6	0.617	2.01	1.65	2.57	3.60	0.884	1.75	0.549
1 212.0	0.575	1.88	1.57	2.41	3.39	0.830	1.64	0.524
1 339.4	0.536	1.76	1.48	2.27	3.19	0.778	1.55	0.500
1 480.3	0.498	1.64	1.40	2.12	3.00	0.728	1.45	0.476
1 636.0	0.463	1.53	1.32	1.99	2.81	0.680	1.36	0.452
1 808.0	0.430	1.43	1.24	1.86	2.63	0.635	1.27	0.428
1 998.2	0.399	1.33	1.16	1.74	2.46	0.592	1.19	0.405
2 208.3	0.370	1.23	1.09	1.62	2.30	0.551	1.11	0.382
2 440.6	0.343	1.15	1.01	1.51	2.14	0.513	1.03	0.359
2 697.3	0.317	1.06	0.948	1.40	2.00	0.476	0.959	0.338
2 981.0	0.294	0.986	0.885	1.30	1.86	0.443	0.891	0.317
3 294.5	0.271	0.914	0.824	1.21	1.73	0.412	0.828	0.297
3 640.9	0.251	0.846	0.767	1.12	1.61	0.384	0.769	0.278
4 023.9	0.232	0.783	0.712	1.04	1.49	0.357	0.715	0.260
4 447.1	0.214	0.724	0.662	0.966	1.38	0.333	0.665	0.242
4 914.8	0.197	0.669	0.614	0.895	1.28	0.309	0.618	0.226
5 431.7	0.182	0.618	0.569	0.828	1.19	0.288	0.574	0.210
6 002.9	0.168	0.571	0.527	0.766	1.10	0.267	0.533	0.195
6 634.2	0.155	0.527	0.488	0.708	1.02	0.248	0.495	0.182
7 332.0	0.143	0.486	0.452	0.654	0.940	0.230	0.459	0.169
8 103.1	0.131	0.448	0.418	0.604	0.868	0.213	0.426	0.156
8 955.3	0.121	0.413	0.386	0.557	0.802	0.197	0.394	0.145
9 897.1	0.111	0.381	0.356	0.514	0.740	0.183	0.365	0.134
10 938.0	0.102	0.351	0.329	0.474	0.683	0.169	0.338	0.124
12 088.4	0.0943	0.323	0.304	0.437	0.630	0.156	0.312	0.115
13 359.7	0.0867	0.297	0.280	0.402	0.580	0.144	0.289	0.106
14 764.8	0.0797	0.273	0.258	0.370	0.535	0.133	0.267	0.0985
16 317.6	0.0733	0.251	0.238	0.341	0.492	0.123	0.246	0.0911
18 033.7	0.0673	0.231	0.219	0.314	0.453	0.113	0.227	0.0843
19 930.4	0.0619	0.213	0.202	0.289	0.417	0.105	0.209	0.0780
22 026.5	0.0568	0.195	0.186	0.265	0.384	0.0963	0.193	0.0721
24 343.0	0.0522	0.179	0.171	0.244	0.353	0.0888	0.178	0.0666
26 903.2	0.0479	0.165	0.157	0.224	0.325	0.0817	0.164	0.0615
29 732.6	0.0440	0.151	0.144	0.206	0.298	0.0752	0.151	0.0568

TABLE I. (*Continued.*)

	Stopping power (eV/Å)							
E (eV)	Sc	Ti	V	Fe	Y	Zr	Nb	Mo
99.5	7.18	5.59	5.55	6.85	5.63	6.51	6.02	8.42
109.9	7.25	6.03	5.59	7.05	5.70	6.50	6.19	8.69
121.5	7.21	6.26	5.59	7.25	5.70	6.42	6.28	8.91
134.3	7.10	6.35	5.56	7.40	5.64	6.30	6.30	9.03
148.4	6.94	6.35	5.50	7.52	5.52	6.16	6.27	9.05
164.0	6.74	6.29	5.42	7.57	5.37	6.01	6.18	8.97
181.3	6.52	6.18	5.33	7.60	5.19	5.82	6.04	8.81
200.3	6.28	6.04	5.23	7.59	5.00	5.61	5.88	8.57
221.4	6.03	5.87	5.11	7.56	4.79	5.38	5.69	8.29
244.7	5.77	5.69	4.97	7.49	4.58	5.15	5.48	7.98
270.4	5.50	5.50	4.82	7.38	4.37	4.92	5.27	7.65
298.9	5.24	5.29	4.67	7.25	4.16	4.69	5.04	7.31
330.3	4.98	5.07	4.50	7.08	3.95	4.45	4.81	6.96
365.0	4.72	4.86	4.33	6.90	3.76	4.23	4.59	6.62
403.4	4.47	4.64	4.16	6.70	3.57	4.01	4.36	6.28
445.9	4.22	4.42	3.98	6.47	3.40	3.80	4.14	5.95
492.7	3.98	4.20	3.81	6.24	3.24	3.61	3.93	5.62
544.6	3.75	3.98	3.63	5.99	3.09	3.43	3.73	5.32
601.8	3.52	3.77	3.45	5.74	2.96	3.28	3.55	5.04
665.1	3.31	3.56	3.27	5.48	2.84	3.13	3.40	4.80
735.1	3.10	3.36	3.10	5.22	2.73	3.00	3.27	4.58
812.4	2.90	3.16	2.93	4.96	2.62	2.88	3.15	4.38
897.8	2.72	2.98	2.77	4.70	2.51	2.77	3.05	4.20
992.3	2.55	2.79	2.61	4.45	2.41	2.66	2.95	4.03
1 096.6	2.41	2.62	2.45	4.20	2.31	2.55	2.84	3.86
1 212.0	2.27	2.48	2.31	3.96	2.21	2.45	2.75	3.71
1 339.4	2.15	2.35	2.19	3.73	2.11	2.35	2.65	3.56
1 480.3	2.03	2.23	2.09	3.50	2.01	2.25	2.55	3.41
1 636.0	1.92	2.12	2.00	3.29	1.91	2.15	2.45	3.27
1 808.0	1.81	2.01	1.91	3.08	1.82	2.04	2.35	3.12
1 998.2	1.70	1.91	1.82	2.90	1.72	1.94	2.24	2.98
2 208.3	1.60	1.80	1.74	2.75	1.63	1.85	2.14	2.83
2 440.6	1.50	1.70	1.66	2.60	1.53	1.75	2.04	2.69
2 697.3	1.41	1.61	1.57	2.46	1.45	1.65	1.94	2.55
2 981.0	1.32	1.51	1.49	2.32	1.36	1.56	1.84	2.41
3 294.5	1.23	1.42	1.41	2.19	1.28	1.47	1.74	2.28
3 640.9	1.15	1.33	1.33	2.07	1.20	1.38	1.64	2.15
4 023.9	1.08	1.25	1.25	1.94	1.12	1.30	1.54	2.02
4 447.1	1.00	1.17	1.18	1.83	1.05	1.22	1.45	1.90
4 914.8	0.933	1.09	1.11	1.71	0.976	1.14	1.36	1.78
5 431.7	0.868	1.02	1.04	1.60	0.910	1.06	1.28	1.67
6 002.9	0.806	0.948	0.969	1.50	0.848	0.993	1.19	1.56
6 634.2	0.748	0.882	0.905	1.40	0.790	0.926	1.11	1.45
7 332.0	0.694	0.820	0.845	1.31	0.737	0.865	1.04	1.36
8 103.1	0.643	0.762	0.787	1.22	0.688	0.808	0.973	1.26
8 955.3	0.596	0.707	0.733	1.13	0.642	0.756	0.911	1.18
9 897.1	0.551	0.656	0.681	1.05	0.598	0.706	0.852	1.10
10 938.0	0.510	0.608	0.633	0.980	0.557	0.660	0.797	1.03
12 088.4	0.471	0.563	0.587	0.910	0.519	0.615	0.745	0.959
13 359.7	0.436	0.521	0.545	0.844	0.482	0.574	0.696	0.897
14 764.8	0.402	0.482	0.505	0.782	0.448	0.534	0.649	0.835
16 317.6	0.371	0.446	0.467	0.724	0.416	0.497	0.605	0.778
18 033.7	0.343	0.412	0.433	0.670	0.386	0.462	0.563	0.723
19 930.4	0.317	0.381	0.400	0.620	0.358	0.429	0.524	0.672
22 026.5	0.292	0.352	0.370	0.573	0.332	0.398	0.487	0.624
24 343.0	0.270	0.325	0.343	0.529	0.307	0.369	0.452	0.579
26 903.2	0.249	0.300	0.317	0.488	0.284	0.342	0.419	0.537
29 732.6	0.230	0.277	0.293	0.451	0.262	0.317	0.388	0.497

TABLE I. (*Continued.*)

	Stopping power (eV/Å)							
E (eV)	Ru	Rh	In	Sn	Cs	Gd	Tb	Dy
99.5	9.05	8.81	4.59	3.93	1.50	6.28	7.86	7.42
109.9	9.53	9.34	4.83	4.14	1.44	6.26	7.96	7.55
121.5	9.89	9.81	5.07	4.39	1.37	6.22	7.96	7.61
134.3	10.1	10.4	5.31	4.68	1.30	6.14	7.90	7.59
148.4	10.2	10.8	5.56	4.97	1.24	6.02	7.79	7.52
164.0	10.2	11.0	5.81	5.25	1.19	5.90	7.64	7.42
181.3	10.0	11.0	6.03	5.50	1.18	5.74	7.45	7.28
200.3	9.76	10.8	6.19	5.71	1.19	5.58	7.24	7.12
221.4	9.44	10.5	6.24	5.84	1.22	5.41	7.02	6.93
244.7	9.08	10.1	6.20	5.87	1.26	5.22	6.77	6.73
270.4	8.71	9.76	6.09	5.82	1.28	5.02	6.51	6.50
298.9	8.32	9.36	5.92	5.71	1.27	4.85	6.25	6.26
330.3	7.93	8.94	5.71	5.54	1.25	4.80	6.08	6.09
365.0	7.54	8.52	5.48	5.34	1.21	4.71	5.90	5.94
403.4	7.15	8.10	5.24	5.12	1.16	4.61	5.72	5.78
445.9	6.78	7.69	4.99	4.89	1.11	4.48	5.52	5.60
492.7	6.41	7.29	4.74	4.67	1.06	4.34	5.31	5.41
544.6	6.06	6.89	4.50	4.44	1.00	4.19	5.10	5.21
601.8	5.72	6.51	4.27	4.22	0.953	4.03	4.89	5.01
665.1	5.40	6.14	4.04	4.00	0.903	3.87	4.67	4.80
735.1	5.09	5.79	3.82	3.79	0.855	3.70	4.46	4.59
812.4	4.80	5.46	3.61	3.58	0.809	3.54	4.25	4.39
897.8	4.55	5.16	3.40	3.38	0.764	3.37	4.04	4.18
992.3	4.32	4.92	3.21	3.19	0.721	3.21	3.84	3.98
1 096.6	4.12	4.70	3.02	3.00	0.680	3.05	3.64	3.79
1 212.0	3.96	4.51	2.85	2.83	0.641	2.90	3.45	3.60
1 339.4	3.81	4.33	2.71	2.67	0.603	2.75	3.26	3.41
1 480.3	3.66	4.16	2.57	2.54	0.567	2.60	3.08	3.23
1 636.0	3.52	3.99	2.45	2.41	0.532	2.46	2.91	3.05
1 808.0	3.38	3.83	2.34	2.30	0.499	2.32	2.74	2.88
1 998.2	3.24	3.66	2.23	2.19	0.472	2.19	2.58	2.71
2 208.3	3.10	3.50	2.12	2.09	0.448	2.06	2.42	2.55
2 440.6	2.96	3.33	2.02	1.99	0.426	1.94	2.28	2.40
2 697.3	2.82	3.17	1.92	1.89	0.404	1.82	2.13	2.25
2 981.0	2.67	3.01	1.83	1.80	0.384	1.70	2.00	2.11
3 294.5	2.53	2.85	1.73	1.70	0.365	1.60	1.87	1.98
3 640.9	2.40	2.69	1.64	1.61	0.346	1.51	1.75	1.85
4 023.9	2.26	2.53	1.54	1.52	0.328	1.42	1.65	1.74
4 447.1	2.13	2.39	1.46	1.43	0.310	1.34	1.55	1.63
4 914.8	2.00	2.24	1.37	1.35	0.293	1.27	1.46	1.54
5 431.7	1.88	2.10	1.28	1.27	0.276	1.20	1.37	1.45
6 002.9	1.76	1.97	1.20	1.19	0.260	1.13	1.29	1.36
6 634.2	1.65	1.84	1.13	1.11	0.244	1.07	1.21	1.28
7 332.0	1.54	1.72	1.05	1.04	0.229	1.01	1.14	1.20
8 103.1	1.43	1.60	0.984	0.973	0.215	0.948	1.07	1.12
8 955.3	1.34	1.49	0.918	0.908	0.201	0.890	0.998	1.05
9 897.1	1.25	1.39	0.855	0.846	0.188	0.834	0.933	0.984
10 938.0	1.16	1.30	0.795	0.788	0.175	0.781	0.871	0.920
12 088.4	1.09	1.21	0.739	0.732	0.163	0.731	0.813	0.858
13 359.7	1.01	1.13	0.687	0.681	0.152	0.682	0.757	0.800
14 764.8	0.946	1.05	0.640	0.633	0.142	0.636	0.705	0.745
16 317.6	0.882	0.978	0.595	0.588	0.132	0.593	0.655	0.693
18 033.7	0.821	0.910	0.553	0.547	0.122	0.552	0.609	0.644
19 930.4	0.763	0.846	0.514	0.509	0.113	0.513	0.565	0.598
22 026.5	0.709	0.786	0.477	0.472	0.105	0.477	0.524	0.554
24 343.0	0.659	0.729	0.443	0.438	0.0980	0.442	0.485	0.514
26 903.2	0.611	0.676	0.411	0.407	0.0910	0.410	0.450	0.476
29 732.6	0.566	0.627	0.381	0.377	0.0844	0.380	0.416	0.440

TABLE I. (*Continued.*)

	Stopping power (eV/Å)						
E (eV)	Hf	Ta	W	Re	Os	Ir	Bi
99.5	5.05	7.92	9.97	10.7	9.49	9.36	4.77
109.9	5.16	8.39	10.3	11.7	10.0	9.71	5.03
121.5	5.24	8.78	10.5	12.6	10.4	9.94	5.31
134.3	5.29	9.02	10.6	13.3	10.8	10.1	5.58
148.4	5.30	9.13	10.6	13.8	11.0	10.1	5.79
164.0	5.28	9.14	10.5	14.0	11.1	10.1	6.00
181.3	5.24	9.09	10.3	14.1	11.1	9.99	6.10
200.3	5.19	9.00	10.2	14.0	11.0	9.86	6.17
221.4	5.13	8.88	10.0	13.8	10.8	9.69	6.15
244.7	5.05	8.71	9.79	13.5	10.7	9.51	6.08
270.4	4.97	8.54	9.55	13.2	10.4	9.29	5.97
298.9	4.89	8.34	9.31	12.8	10.2	9.06	5.82
330.3	4.80	8.14	9.05	12.4	9.96	8.82	5.62
365.0	4.72	7.93	8.79	12.0	9.69	8.58	5.42
403.4	4.63	7.71	8.54	11.6	9.42	8.34	5.19
445.9	4.55	7.49	8.29	11.2	9.14	8.09	4.96
492.7	4.46	7.27	8.04	10.8	8.87	7.85	4.74
544.6	4.36	7.05	7.80	10.4	8.60	7.61	4.51
601.8	4.26	6.84	7.56	10.1	8.33	7.38	4.30
665.1	4.16	6.62	7.33	9.70	8.07	7.16	4.10
735.1	4.05	6.39	7.09	9.33	7.80	6.94	3.91
812.4	3.94	6.17	6.85	8.98	7.55	6.74	3.74
897.8	3.82	5.94	6.61	8.62	7.29	6.54	3.57
992.3	3.70	5.72	6.37	8.27	7.03	6.33	3.42
1 096.6	3.58	5.50	6.13	7.92	6.78	6.12	3.27
1 212.0	3.46	5.27	5.89	7.57	6.52	5.91	3.14
1 339.4	3.33	5.06	5.66	7.24	6.27	5.70	3.00
1 480.3	3.20	4.84	5.42	6.90	6.01	5.49	2.87
1 636.0	3.07	4.62	5.19	6.58	5.76	5.28	2.74
1 808.0	2.94	4.41	4.95	6.27	5.51	5.07	2.62
1 998.2	2.81	4.19	4.72	5.95	5.27	4.86	2.50
2 208.3	2.68	3.98	4.49	5.65	5.02	4.64	2.39
2 440.6	2.55	3.78	4.26	5.35	4.77	4.43	2.28
2 697.3	2.42	3.57	4.04	5.06	4.53	4.22	2.17
2 981.0	2.29	3.38	3.82	4.77	4.30	4.01	2.06
3 294.5	2.17	3.18	3.61	4.50	4.06	3.80	1.95
3 640.9	2.05	3.00	3.40	4.23	3.83	3.59	1.85
4 023.9	1.93	2.82	3.20	3.97	3.61	3.39	1.74
4 447.1	1.81	2.65	3.01	3.73	3.40	3.20	1.64
4 914.8	1.70	2.48	2.82	3.49	3.19	3.01	1.55
5 431.7	1.61	2.33	2.64	3.27	3.00	2.83	1.45
6 002.9	1.52	2.19	2.49	3.06	2.81	2.65	1.36
6 634.2	1.44	2.06	2.34	2.87	2.64	2.49	1.27
7 332.0	1.36	1.94	2.21	2.70	2.48	2.35	1.19
8 103.1	1.28	1.83	2.08	2.53	2.33	2.21	1.11
8 955.3	1.21	1.72	1.95	2.38	2.20	2.09	1.04
9 897.1	1.14	1.61	1.83	2.23	2.06	1.97	0.975
10 938.0	1.07	1.51	1.72	2.09	1.94	1.85	0.912
12 088.4	1.01	1.42	1.61	1.95	1.82	1.73	0.854
13 359.7	0.942	1.33	1.51	1.83	1.70	1.63	0.798
14 764.8	0.882	1.24	1.41	1.70	1.59	1.53	0.751
16 317.6	0.825	1.16	1.32	1.59	1.49	1.43	0.701
18 033.7	0.770	1.08	1.23	1.48	1.39	1.34	0.653
19 930.4	0.718	1.00	1.15	1.38	1.29	1.25	0.607
22 026.5	0.669	0.934	1.07	1.28	1.20	1.16	0.565
24 343.0	0.623	0.868	0.991	1.19	1.12	1.08	0.526
26 903.2	0.579	0.806	0.921	1.10	1.04	1.01	0.489
29 732.6	0.538	0.748	0.854	1.02	0.967	0.937	0.453

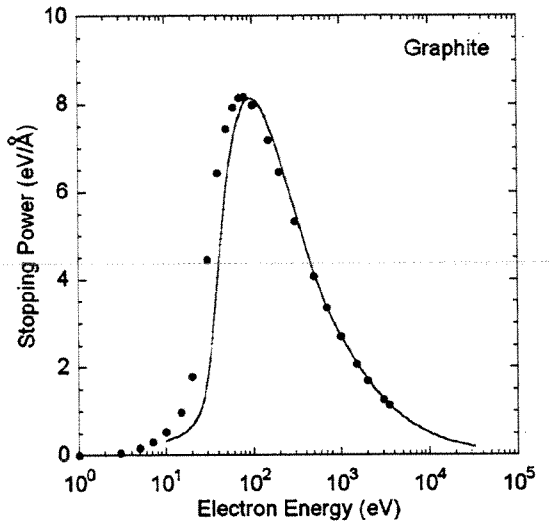

FIG. 7. Comparison of calculated SPs for graphite (solid line) with values derived from electron energy-loss measurements (solid circles) (Ref. 26) as a function of electron kinetic energy E.

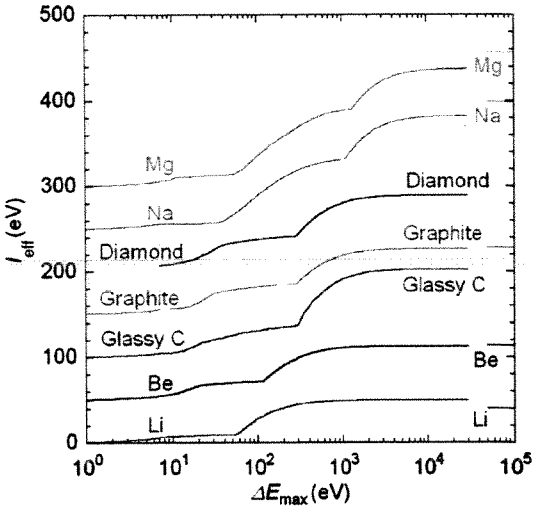

FIG. 8. (Color online) Plot of the effective MEE I_{eff} as a function of the maximum excitation energy ΔE_{max} for Li, Be, glassy carbon, graphite, diamond, Na, and Mg. The horizontal lines on the right ordinate axis indicate values of the MEE recommended in Ref. 1. For clarity, the plots and the horizontal lines for Be and successive elements have been displaced upward in increments of 50 eV.

values. Sorini *et al.*[27] recently reported SPs for Cu, Ag, and Au from a first-principles calculation of the complex dielectric function and then the ELF. Agreement within about 10% was found between their SPs and our results for Cu (for $E>400$ eV), Ag (for $E>200$ eV), and Au (for $E>200$ eV). Although the Ashley and Ochkur[24] exchange corrections lead to decreases in calculated SPs for a group of ten organic solids of up to about 29% at 100 eV,[25] more detailed comparisons of calculated and measured SPs are needed to assess the reliability of these calculations.

Evaluation of MEEs

Shiles *et al.*[33] showed that values of the MEE for solids could be obtained by integration of the ELF,

$$\ln I = \frac{\int_0^\infty \Delta E \ln(\Delta E)\mathrm{Im}[\varepsilon^{-1}(\Delta E)]d(\Delta E)}{\int_0^\infty \Delta E\, \mathrm{Im}[\varepsilon^{-1}(\Delta E)]d(\Delta E)}, \quad (7)$$

where $\Delta E=\hbar\omega$ is the excitation energy. They also determined an effective MEE, I_{eff}, for Al as a function of the maximum excitation energy ΔE_{max} by using this parameter instead of infinity as the upper limit in the integrations of Eq. (7),

$$\ln I_{eff} = \frac{\int_0^{\Delta E_{max}} \Delta E \ln(\Delta E)\mathrm{Im}[\varepsilon^{-1}(\Delta E)]d(\Delta E)}{\int_0^{\Delta E_{max}} \Delta E\, \mathrm{Im}[\varepsilon^{-1}(\Delta E)]d(\Delta E)}. \quad (8)$$

Figures 8–13 show plots of I_{eff} as a function of ΔE_{max} for each of our 41 elemental solids. These plots are useful in that they show the relative contributions of valence-electron excitations and core-electron excitations to the MEE. For example, Fig. 8 indicates that the contribution of valence-electron excitations to the MEE is much less than that of core-electron excitations. We also see the onset of K-shell contributions to the MEE for Li through Mg that begin at the K-shell ionization energies. These thresholds shift systematically with Z as expected. The onset of L-shell excitations is seen for Na and Mg in Fig. 8. These trends continue in Figs. 9–13 where onsets for M-shell and N-shell excitations are seen. The similar shapes of the I_{eff} plots for elements of similar Z are reasonable because the ELF is proportional to the x-ray absorption coefficient and is mainly determined by atomic properties for ΔE_{max} larger than about 100 eV (with the exception of structure near x-ray absorption edges and weak extended-x-ray-absorption-fine-structure-type oscillations).

While most of the trends with Z in Figs. 8–13 appear qualitatively reasonable, there are some quantitative anomalies. In particular, the "saturation" values of I_{eff} for ΔE_{max}

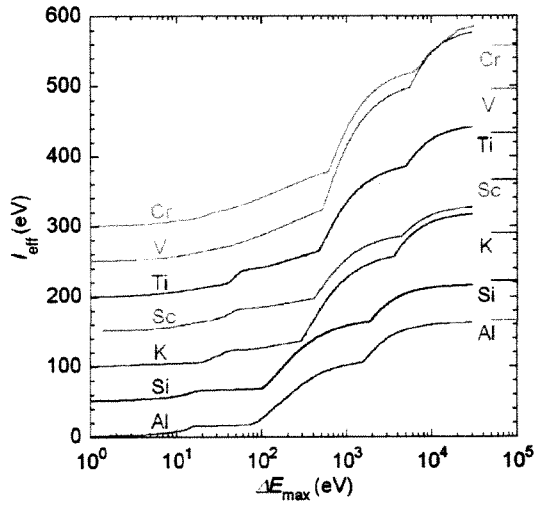

FIG. 9. (Color online) Same as Fig. 8 except for Al, Si, K, Sc, Ti, V, and Cr.

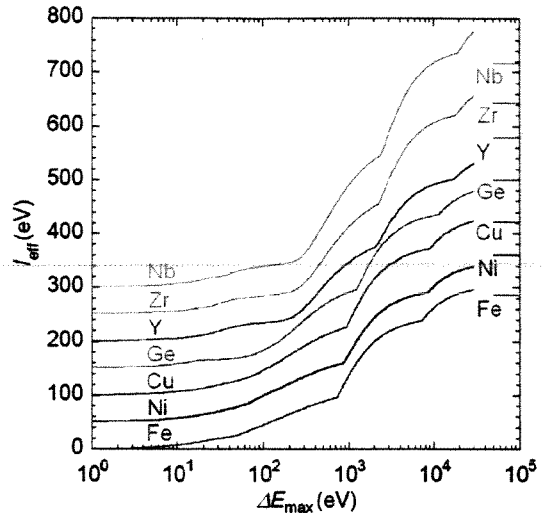

FIG. 10. (Color online) Same as Fig. 8 except for Fe, Ni, Cu, Ge, Y, Zr, and Nb.

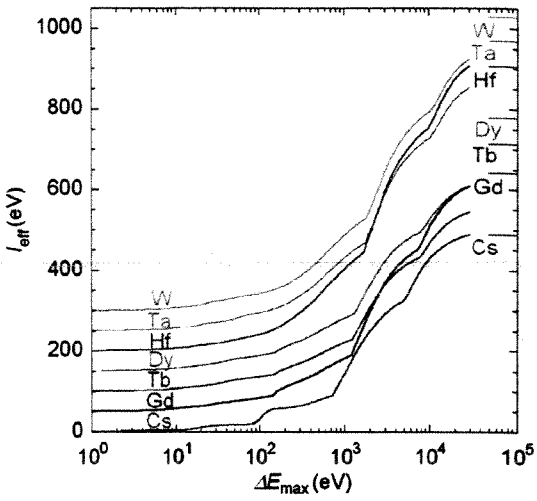

FIG. 12. (Color online) Same as Fig. 8 except for Cs, Gd, Tb, Dy, Hf, Ta, and W.

=30 keV are sometimes substantially higher or lower than the recommended MEE values of Ref. 1, indicated by the horizontal lines on the right ordinate axes of Figs. 8–13. For example, the saturation values of I_{eff} for K, V, and Cr in Fig. 9 are larger than the recommended MEE values in Fig. 9, while the I_{eff} value for Sc is smaller than the recommended value. Similar disagreements occur for Zr and Nb in Fig. 10, for Ru, Pd, Ag, In, and Sn in Fig. 11, for Tb, Dy, and Hf in Fig. 12, and for many of the elements in Fig. 13. Nevertheless, we do not expect correspondence between our saturation values of I_{eff} at ΔE_{max}=30 keV for $Z \geqslant 51$ (Sb) because our limit would then be smaller than the K-shell binding energy. In addition, we can see from the I_{eff} plots for Li–Si in Figs. 8 and 9 that ΔE_{max} should be appreciably larger than the K-shell binding energy (by roughly an order of magnitude) in order for I_{eff} to reach its saturation value. It is then only reasonable to make a detailed comparison of our saturation values of I_{eff} with the recommended MEEs of Ref. 1 for Z less than about 21.

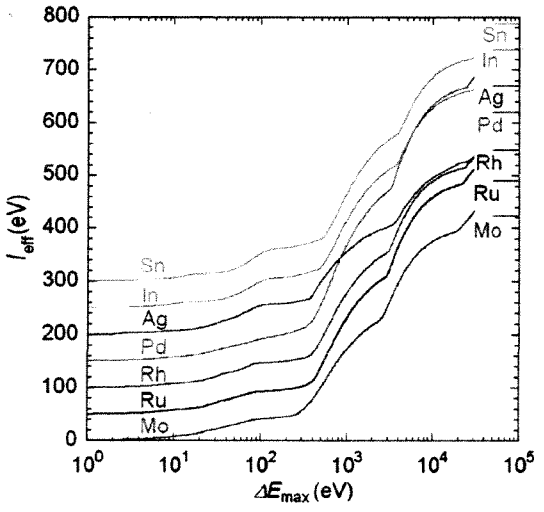

FIG. 11. (Color online) Same as Fig. 8 except for Mo, Ru, Rh, Pd, Ag, In, and Sn.

We also point out that an important reason for the quantitative discrepancies between our saturation values of I_{eff} and the recommended MEE values from Ref. 1 in Figs. 8–13 is that values of I_{eff} from Eq. (8) can have substantial uncertainties. For example, a 1% uncertainty in $\ln(I_{eff})$ will lead to uncertainties in I_{eff} between 3.8% (for I_{eff}=40 eV) and 7.2% (for I_{eff}=1000 eV). Similarly, a 5% uncertainty in $\ln(I_{eff})$ will lead to uncertainties in I_{eff} between 20.2% (for I_{eff}=40 eV) and 41.3% (for I_{eff}=1000 eV). While the plots of Figs. 8–13 are useful in showing the relative contributions of different shells to I_{eff} for each solid, we need to consider how uncertainties in the ELFs from optical data can affect the derived values of I_{eff}.

It is useful to evaluate the denominator in Eq. (8) which is proportional to the oscillator sum or f-sum for the ELF,[18]

$$Z_{eff} = (2/\pi\hbar^2\Omega_p^2)\int_0^{\Delta E_{max}} \Delta E \, \mathrm{Im}[\varepsilon^{-1}(\Delta E)]d(\Delta E), \qquad (9)$$

where $\Omega_p=(4\pi Ne^2/m_0)^{1/2}$. In the limit $\Delta E_{max}\rightarrow\infty$, Z_{eff} should become equal to Z. Figure 14 shows plots of Z_{eff} as a

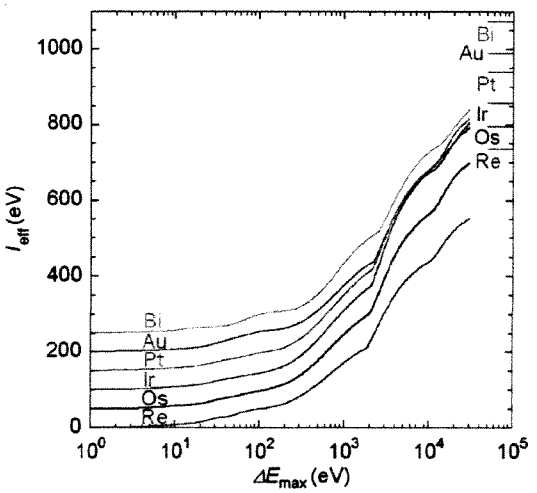

FIG. 13. (Color online) Same as Fig. 8 except for Re, Os, Ir, Pt, Au, and Bi.

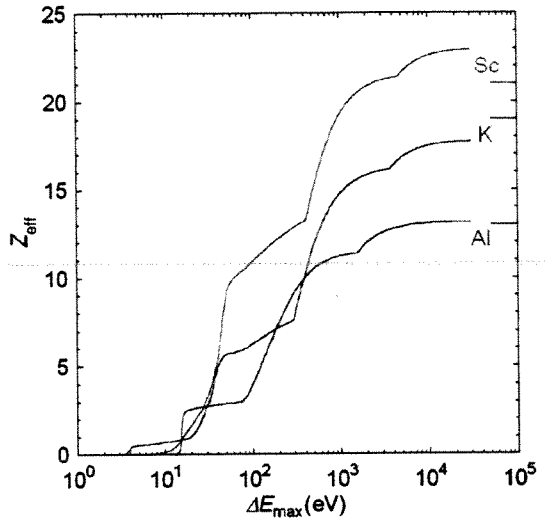

FIG. 14. (Color online) Plot of Z_{eff} from Eq. (9) as a function of ΔE_{max} for Al, K, and Sc. The horizontal lines on the right ordinate axis indicate the values of Z for each solid.

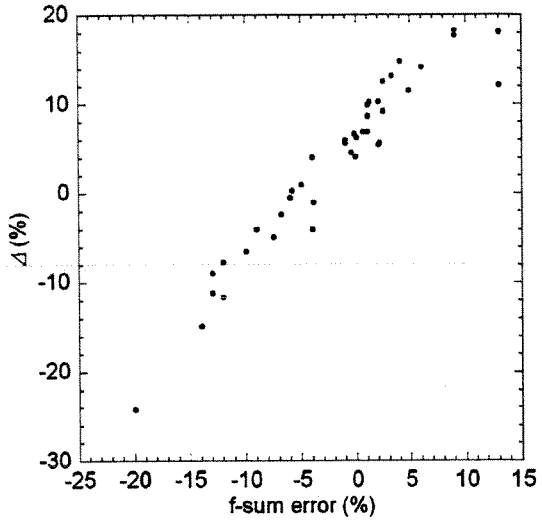

FIG. 15. Plot of Δ, the percentage difference between the SP calculated from optical data at an energy $E=29.733$ keV for each solid and the corresponding SP from the Bethe equation [Eq. (5)] vs the f-sum error from Eq. (9) with $\Delta E_{max}=30$ keV.

function of ΔE_{max} from Eq. (9) for Al, K, and Sc; the corresponding values of Z (13, 19, and 21, respectively) are indicated by the horizontal lines on the right ordinate axis. These three solids were selected for examination because the saturation value of I_{eff} in Fig. 9 for Al was approximately equal to the recommended MEE of Ref. 1, the value of I_{eff} for K was larger than the recommended MEE, and the value of I_{eff} for Sc was smaller than the recommended MEE. The saturation values of Z_{eff} from Fig. 14 are 13.13, 17.72, and 22.90 for Al, K, and Sc, respectively, and the corresponding errors in the f-sum are 1.0%, −6.8%, and 9.0%.[17]

Comparisons of the Z_{eff} plots in Fig. 14 indicate that the f-sum errors for K and Sc appear to arise mainly from an underestimate for K and an overestimate for Sc of the M-shell contributions to Z_{eff}. Similar f-sum errors appear to be mainly responsible for the differences between the saturation values of I_{eff} for K and Sc and the corresponding recommended MEEs from Ref. 1. We think it likely that the substantial ELF f-sum errors for some other solids[16] in our group of 41 elements [specifically V (−20%), Cr (−13%), Zr (−12%), Nb (−14%), Mo (−10%), Ru (−13%), Pd (−12%), Ag (9%), and Au (13%)] are partly responsible for the larger numerical differences between the saturation values of I_{eff} in Figs. 8–13 and the recommended MEEs of Ref. 1. As already discussed, the saturation values of I_{eff} are expected to be less than the recommended MEEs for Z greater than about 22 since our largest value of ΔE_{max} (30 keV) is not large enough to include fully the contributions to I_{eff} from K-shell excitations for medium- and high-Z elements and from L-shell excitations for high-Z elements.

Despite the numerical discrepancies between our saturation values of I_{eff} and the recommended MEEs of Ref. 1 in Figs. 8–13, the SPs calculated from optical data in Figs. 1–6 agree reasonably with values obtained from the Bethe SP equation [Eq. (5) with the recommended MEEs]. The root-mean-square (rms) deviation between the calculated SPs and the values from Eq. (5) were 11.4% and 10.2% at energies $E=9.897$ keV and $E=29.733$ keV, respectively. Figures 8–13 indicate that inner-shell excitations contribute more to the SP than valence-shell excitations, as expected from the weighting of the ELF by the excitation energy in the SP calculation [Eq. (3)]. We therefore consider the hypothesis that the percentage deviation Δ between the calculated SP for each solid at 29.733 keV and the corresponding value from Eq. (5) is mainly associated with the f-sum error [from Eq. (9) with $\Delta E_{max}=30$ keV].[16,17] Although K-shell and some L-shell excitations are not included in the determination of Z_{eff} for high-Z elements, Fig. 15 shows a clear correlation between Δ and the f-sum error for the 41 elemental solids. There is one outlier (Au) in Fig. 15 for which the f-sum error is 13%. This outlier is probably due to errors in the ELF distribution (i.e., the optical data) for Au. We also point out that the rms deviation of 10.2% between our SPs and values from Eq. (5) at 29.733 keV is only slightly larger than the rms f-sum error of 7.9%. It is clear that higher-quality optical data are needed for some solids to obtain more reliable SPs and MEEs.

We now compare our saturation values of I_{eff} with the recommended MEE values of Ref. 1 for solids with $Z<22$ and with f-sum errors between −5% and 5%. These restrictions are made since, as discussed above, the contributions of K-shell excitations to I_{eff} are included (Figs. 8 and 9) and the ELFs, in the region of large excitation energies relevant to the SP calculations, are of better accuracy (Fig. 15). The solids satisfying these criteria are listed in Table II. We see reasonably close agreement between our saturation values of I_{eff} and the recommended MEEs for all elements except Li.

Lithium is a very reactive metal, and it seems likely that the 25% difference between our saturation I_{eff} value and the MEE from Ref. 1 is that sample oxidation could have affected either or both of the measurements. The recommended MEE is based on SP measurements for ~300 MeV protons in thin Li films;[34] unfortunately, no information is given on film preparation and on any protective layer that might have been used. The Li ELF was determined from recommended

TABLE II. Comparison of MEEs for solid and atomic Be, Li, C, Na, Al, and Si.

	I (eV)				
	Solid				Atomic
Element	This work	ICRU Report[a]	Smith *et al.*[b]	Fernandez-Varea *et al.*[c]	
Li	49.8	40			33.3[d]
					34.0[e]
Be	62.9	63.7			38.6[e]
Glassy C	102.5				
Graphite	76.5	78	77		62[e]
Diamond	89.4				
Na	132.2	149			130[d]
					123.6[e]
Al	162.1	166	165.7	164	124.3[e]
Si	165.9	173	164	174	131.5[e]

[a]Reference 1.
[b]Reference 38.
[c]Reference 23.
[d]Reference 40.
[e]Reference 42.

optical data,[35] based on one set of measurements[36] for photon energies between 0.14 and 10.6 eV and photoabsorption data[21] for energies between 30 eV and 30 keV; the ELF was interpolated between 10.6 and 30 eV with a ΔE^n equation. The former data set[36] was based on reflectance measurements on films prepared in ultrahigh vacuum and the latter data set[21] was derived from multiple sources. Tests of ELFs for Al, Si, Ti, Mo, W, and Ir with the f-sum rule and a related sum rule (an integral of the ELF times ΔE^{-1}) have proven useful in identifying oxidation of the samples in optical measurements;[18] no evidence for oxidation was found in the Li ELF data set. Finally, we point out that the value of I/Z for Li from Ref. 1 is 16% less than the corresponding value for Be and 36% less than the value for He. Such a discontinuity is not expected from theory.[37] We conclude that our saturation value of I_{eff} for Li of 49.8 eV is better for the MEE than the value of I in Ref. 1 of 40 eV.

Table II also shows comparisons of our saturation values of I_{eff} with MEE values determined in a similar way by Smith *et al.*[38] and Fernandez-Varea *et al.*[23] for graphite, Al, and Si. There is good agreement among the three sources for graphite and Al but, for Si, Fernandez-Varea *et al.* find a larger MEE (174 eV) than Smith *et al.* (164 eV) or us (165.9 eV). Fernandez-Varea *et al.* utilized a set of optical data from Bichsel[39] who combined and adjusted measured and calculated optical data to satisfy optical sum rules and to obtain $I=174$ eV, a value he had obtained from proton SP measurements. The discrepancy between the recommended MEE for Si in Ref. 1 (173 ± 3 eV) was discussed by Smith *et al.*[38] who pointed out that the near equality of the MEEs for Al and Si is due to the dominant contributions of K- and L-shell excitations to the MEE, as shown in Fig. 9. While the K- and L-shell binding energies for Si are larger than the corresponding values for Al, there is little change in the distributions of contributions of these shells in the plots of I_{eff} versus ΔE_{max} for these solids, and so there is little change in the MEE.

Kamakura *et al.*[40] recently reported MEE calculations for 32 gaseous atoms (with $Z \leq 18$) and molecules (containing atoms with $Z \leq 17$) from oscillator-strength spectra published by Berkowitz.[41] Photoabsorption cross sections were analyzed by Berkowitz and further by Kamakura *et al.* so that the f-sum rule and another sum rule on the oscillator-strength distribution were satisfied to $\pm 1\%$. They then determined MEEs from an equation analogous to Eq. (8). Table II shows a comparison of their MEE values for atomic Li and Na with our saturation values of I_{eff} and the recommended MEEs of Ref. 1 for the elemental solids. Similar comparisons are made with MEEs for atomic Be, C, Al, and Si determined from calculations of oscillator strengths using a Hartree–Slater model.[42] Kamakura *et al.*[40] pointed out that MEEs for solids are generally larger than the corresponding values for atoms, and the MEE data in Table II are consistent with this expectation.

The saturation I_{eff} values for glassy C, graphite, and diamond in Table II are clearly different. Our saturation I_{eff} value for graphite (76.5 eV) is in good agreement with the recommended value of Ref. 1 (78 eV). The different saturation values of I_{eff} for glassy C (102.5 eV) and diamond (89.4 eV) illustrate the effects of atomic structure on the spectrum of electronic excitations (i.e., the ELF) in each allotrope and thus the MEE. Analogous effects of structure and bonding on MEEs for molecules containing the same atom have been discussed by Kamakura *et al.*[40]

Energy range for validity of the Bethe SP equation

For simplicity, we will analyze our calculated SPs with the nonrelativistic Bethe equation [Eq. (6)] since the differences between SPs from Eqs. (5) and (6) for our 41 solids are less than 1.1% at 30 keV and less than 0.9% at 10 keV. We can determine the energy range over which our calculated SPs are consistent with Eq. (6) using a Fano plot.[43] This type of plot was originally proposed for the analysis of total inelastic-scattering cross sections[15,43] and can be similarly

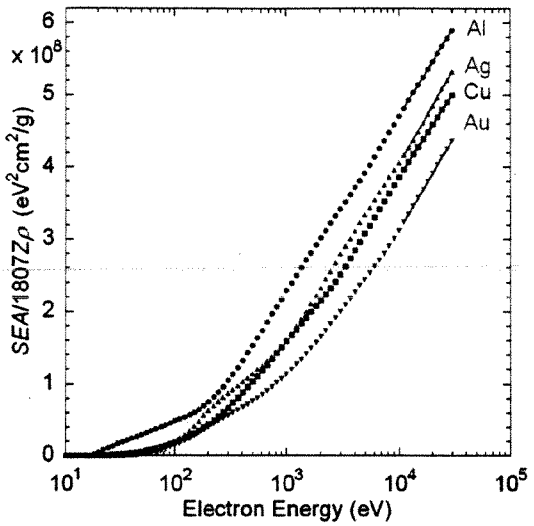

FIG. 16. (Color online) Fano plots (symbols) for Al, Cu, Ag, and Au in which the left-hand side of Eq. (10) is plotted as a function of electron energy E on a logarithmic scale. The solid lines indicate fits with Eq. (10) to each plot for energies between 10 and 30 keV.

used for the analysis of IMFPs (Refs. 16 and 44) and of SP data.[12] If a plot of SE versus $\ln E$ is linear, then the SPs are consistent with Eq. (6).

It is convenient to rewrite Eq. (6) in the following form:

$$\frac{SEA}{1807Z\rho} = \log(1.166/I_F) + m \log E, \tag{10}$$

where I_F and m are parameters to be determined from fits with Eq. (10) for the linear region of a Fano plot. Figure 16 shows Fano plots based on the calculated SPs of Al, Cu, Ag, and Au in which the left-hand side of Eq. (10) is plotted against E on a logarithmic scale. We see that each plot becomes linear for energies above about 10 keV. Satisfactory fits (solid lines in Fig. 16) were made with Eq. (10) for energies between 10 and 30 keV. Ideally, the slopes m for different materials should be unity, but we found slopes of 1.086 ± 0.029, 1.035 ± 0.003, 1.164 ± 0.006, and 1.129 ± 0.002 for Al, Cu, Ag, and Au, respectively (and where the stated uncertainties represent standard deviations). While our calculated SPs are empirically consistent with Eqs. (6) and (10), it is clear that our maximum energy of 30 keV is not high enough for the Fano plot to reach its expected asymptotic slope. Fano plots based on the total ionization cross section[45] of Ar and the total dissociation cross section[46] of CF_4 typically show two linear regions, with the linear region for the higher-energy range showing the expected asymptotic Bethe behavior. Since the Fano plots in Fig. 16 do not show the asymptotic Bethe slope, the values of I_F from the fits (228, 332, 915, and 1654 eV for Al, Cu, Ag, and Au, respectively) are, except for Cu, considerably different from the corresponding recommended MEEs of Ref. 1 of 166, 322, 470, and 790 eV. It is also clear from Fig. 16 that small changes in m [e.g., from selecting different energy regions for fits with Eq. (10)] can lead to substantial uncertainties in values of I_F derived from the intercepts of the lines on the $\log E = 0$ axis.

Finally, we comment on the magnitude of possible errors in SPs from the relativistic Bethe equation [Eq. (4a)] due to the omission of shell corrections. These corrections were introduced to describe the SP reduction when the velocity of the incident electron is not large compared to the velocities of the atomic electrons.[1] A rough estimate has indicated that the shell corrections to the electron SP could be about 4% for Al, 9% for Cu, 12% for Ag, and 21% for Au at an energy of 10 keV.[1] We examined a plot of differences between the SPs computed from optical data and SPs from Eq. (4a) at 9.897 keV as a function of Z, but could not discern any systematic trend. Since the rms f-sum error for our group of 41 solids is 7.4%, we conclude that the shell correction to the SP at 10 keV must be less than about 10%.

SUMMARY

We presented SPs for 100 eV–30 keV electrons in 31 elemental solids (Li, Be, glassy C, graphite, diamond, Na, Mg, K, Sc, Ti, V, Fe, Y, Zr, Nb, Mo, Ru, Rh, In, Sn, Cs, Gd, Tb, Dy, Hf, Ta, W, Re, Os, Ir, and Bi). These SPs were calculated from ELFs derived from experimental optical data using the Penn algorithm.[11] This work supplements a previous report[12] containing SPs for ten additional solids (Al, Si, Cr, Ni, Cu, Ge, Pd, Ag, Pt, and Au) that were calculated by the same approach.

Plots of SP versus Z for each of the 41 solids show clear trends in the shapes of the curves as a function of Z. Multiple peaks and shoulders are seen that result from the contributions of valence-electron excitations and various inner-shell excitations to the total SP. Separate maxima or distinctive shoulders are typically seen for elements with core-electron binding energies less than about 50 eV (such as Na, Ge, In, Sn, Cs, and Bi).

We found that our calculated SPs for the group of 41 solids agreed reasonably with values from the relativistic Bethe SP equation [Eq. (5) and the recommended MEE values from Ref. 1] for energies above 10 keV. At 29.733 keV, the rms deviation between our SPs and values from Eq. (5) was 10.2%. A correlation was found between the deviation for each solid and the f-sum error on the ELF. This correlation indicates that better optical data are needed for some solids to obtain SPs of greater reliability.

We determined values of the effective MEE I_{eff} as a function of maximum excitation energy $\Delta E_{\max}$ for the 41 solids [Eq. (8)]. Plots of I_{eff} versus $\Delta E_{\max}$ showed the relative contributions of valence-electron and core-electron excitations to the MEE. For each solid, the latter contribution was much greater than the former contribution. The saturation values of I_{eff} for $\Delta E_{\max}=30$ keV were sometimes substantially higher or lower than the recommended MEEs of Ref. 1. Inspection of the plots of I_{eff} versus $\Delta E_{\max}$ for Li–Si showed that $\Delta E_{\max}$ should be roughly an order of magnitude larger than the K-shell binding energy in order for I_{eff} to reach its saturation value at $\Delta E_{\max}=30$ keV. It is then only reasonable to compare our saturation values of I_{eff} with the recommended MEEs of Ref. 1 for Z less than about 21. For this low-Z range and for elements with f-sum errors between −5% and 5%, we found reasonably close agreement between

our saturation values of I_{eff} for Be, graphite, Na, Al, and Si and the corresponding recommended MEEs of Ref. 1. For Li, however, there was a substantial difference that we attributed to sample oxidation in the SP measurements of protons in thin Li films that were used to derive the recommended MEE.[1] We also found that our saturation values of I_{eff} for Li, Be, graphite, Na, Al, and Si are larger than the corresponding values for free atoms. Substantially different saturation values of I_{eff} were found for the three carbon allotropes: graphite (76.5 eV), diamond (89.4 eV), and glassy C (102.5 eV). These differences show the effects of atomic structure on the ELF and thus the MEE.

Fano plots for Al, Cu, Ag, and Au show that our calculated SPs are empirically consistent with the nonrelativistic Bethe SP equation for energies between 10 and 30 keV. The parameters derived from fits to these plots with Eq. (10), however, were different from those expected (i.e., our maximum energy of 30 keV was not large enough for the Fano plots to reach the asymptotic Bethe behavior).

ACKNOWLEDGMENTS

The authors thank S. M. Seltzer and C. W. Clark for useful discussions. One of the authors (S.T.) would like to acknowledge the New Energy and Industrial Technology Development Organization for its financial support.

[1]"Stopping Powers for Electrons and Positions," International Commission on Radiation Units and Measurements Report No. 37 (International Commission on Radiation Units and Measurements, Bethesda, 1984.
[2]R. Gauvin, Surf. Interface Anal. **37**, 875 (2005).
[3]N. W. M. Ritchie, Surf. Interface Anal. **37**, 1006 (2005).
[4]F. Salvat, X. Llovet, J. M. Fernandez-Varea, and J. Sempau, Surf. Interface Anal. **37**, 1054 (2005).
[5]A. Jablonski, C. J. Powell, and S. Tanuma, Surf. Interface Anal. **37**, 861 (2005).
[6]J. S. Villarrubia, A. E. Vladar, and M. T. Postek, Surf. Interface Anal. **37**, 951 (2005).
[7]H. Bethe, Ann. Phys. **5**, 325 (1930).
[8]H. Bethe, in *Handbuch der Physik*, edited by H. Geiger and K. Scheel (Springer, Berlin, 1933), Vol. 24/1, p. 273.
[9]H. A. Bethe and J. Ashkin, in *Experimental Nuclear Physics*, edited by E. Segre (Wiley, New York, 1953), p. 166.
[10]M. J. Berger, J. S. Coursey, M. A. Zucker, and J. Chang, "Stopping Power and Range Tables for Electrons, Positrons, and Helium Ions" (http://physics.nist.gov/PhysRefData/Star/Text/contents.html), 2005.
[11]D. R. Penn, Phys. Rev. B **35**, 482 (1987).
[12]S. Tanuma, C. J. Powell, and D. R. Penn, Surf. Interface Anal. **37**, 978 (2005).
[13]C. J. Powell and A. Jablonski, J. Phys. Chem. Ref. Data **28**, 19 (1999).
[14]J. Lindhard, K. Dan. Vidensk. Selsk. Mat. Fys. Medd. **28**, 1 (1954); J. Lindhard and M. Scharff, *ibid.* **27**, 1 (1953); J. Lindhard, M. Scharff, and H. E. Schiott, *ibid.* **33**, 1 (1963).
[15]M. Inokuti, Rev. Mod. Phys. **43**, 297 (1971).
[16]S. Tanuma, C. J. Powell, and D. R. Penn, Surf. Interface Anal. **11**, 577 (1988).
[17]S. Tanuma, C. J. Powell, and D. R. Penn, Surf. Interface Anal. **37**, 1 (2005).
[18]S. Tanuma, C. J. Powell, and D. R. Penn, J. Electron Spectrosc. Relat. Phenom. **62**, 95 (1993).
[19]*Handbook of Optical Constants of Solids III*, edited by E. D. Palik (Academic, San Diego, 1998).
[20]Yu. A. Uspenskii, J. F. Seely, N. L. Popov, A. V. Vinogradov, Yu. P. Pershin, and V. V. Kondratenko, J. Opt. Soc. Am. A **21**, 298 (2004).
[21]B. L. Henke, J. C. Davis, E. M. Gullikson, and R. C. C. Perera, Lawrence Berkely Laboratory Report No. LBL-26259, 1988 (unpublished); B. L. Henke, E. M. Gullikson, and J. C. Davis, At. Data Nucl. Data Tables **54**, 181 (1993).
[22]D. R. Penn, C. W. Clark, C. J. Powell, T. Fulop, and S. Tanuma, Ultramicroscopy **69**, 69 (1997).
[23]J. M. Fernandez-Varea, F. Salvat, M. Dingfelder, and D. Liljequist, Nucl. Instrum. Methods Phys. Res. B **229**, 187 (2005).
[24]V. I. Ochkur, Sov. Phys. JETP **18**, 503 (1964).
[25]Z. Tan, Y. Xia, M. Zhao, X. Liu, F. Li, B. Huang, and Y. Ji, Nucl. Instrum. Methods Phys. Res. B **222**, 27 (2004).
[26]http://physics.nist.gov/cuu/Constants/index.html.
[27]A. P. Sorini, J. J. Kas, J. J. Rehr, M. P. Prange, and Z. H. Levine, Phys. Rev. B **74**, 165111 (2006).
[28]K. Kumagai, S. Tanuma, and C. J. Powell (unpublished).
[29]D. C. Joy, http://web.utk.edu/~srcutk/htm/interact.htm, 2006.
[30]D. C. Joy, S. Luo, R. Gauvin, P. Hovington, and N. Evans, Scanning Microsc. **10**, 653 (1996).
[31]J. C. Ashley, J. Electron Spectrosc. Relat. Phenom. **46**, 199 (1988).
[32]Z. J. Ding and R. Shimizu, Scanning **18**, 92 (1996).
[33]E. Shiles, T. Sasaki, M. Inokuti, and D. Y. Smith, Phys. Rev. B **22**, 1612 (1980).
[34]C. J. Bakker and E. Segre, Phys. Rev. **81**, 489 (1951).
[35]*Handbook of Optical Constants of Solids II*, edited by E. D. Palik (Academic, New York, 1991).
[36]M. Rasigni and G. Rasigni, J. Opt. Soc. Am. **67**, 54 (1977).
[37]M. Inokuti, J. L. Dehmer, T. Baer, and J. D. Hanson, Phys. Rev. A **23**, 95 (1981).
[38]D. Y. Smith, M. Inokuti, W. Karstens, and E. Shiles, Nucl. Instrum. Methods Phys. Res. B **250**, 1 (2006).
[39]H. Bichsel, Rev. Mod. Phys. **60**, 663 (1988).
[40]S. Kamakura, N. Sakamoto, H. Ogawa, H. Tsuchida, and M. Inokuti, J. Appl. Phys. **100**, 064905 (2006).
[41]J. Berkowitz, *Atomic and Molecular Photoabsorption: Absolute Total Cross Sections* (Academic, San Diego, 2002).
[42]J. L. Dehmer, M. Inokuti, and R. P. Saxon, Phys. Rev. A **12**, 102 (1975).
[43]U. Fano, Phys. Rev. **95**, 1198 (1954).
[44]S. Tanuma, C. J. Powell, and D. R. Penn, Surf. Interface Anal. **17**, 911 (1991).
[45]F. J. de Heer and M. Inokuti, in *Electron Impact Ionization*, edited by T. H. Märk and G. H. Dunn (Springer-Verlag, Vienna, 1985), p. 232.
[46]H. F. Winters and M. Inokuti, Phys. Rev. A **25**, 1420 (1982).